INSTITUTE OF PHYSICS PUBLISHING PLASMA PHYSICS AND CONTROLLED FUSION

Plasma Phys. Control. Fusion **43** (2001) A349–A373 PII: S0741-3335(01)28798-3

Hydrogen release from plasma-facing components into fusion plasmas—recent results from a spectroscopic approach

Ph Mertens[1], S Brezinsek[1], P T Greenland[2], J D Hey[3], A Pospieszczyk[1], D Reiter[1], U Samm[1], B Schweer[1], G Sergienko[4], E Vietzke[1]

[1] Institut für Plasmaphysik, Forschungszentrum Jülich GmbH, EURATOM-Association, Trilateral Euregio Cluster, D-52425 Jülich, Germany
[2] Blackett Laboratory, Imperial College, London, UK
[3] Plasma Physics Research Institute, University of Natal, Durban 4041, South Africa
[4] Institute for High Temperatures of the RAS, 'IVTAN' Association, Moscow, Russia

Received 22 June 2001
Published 22 November 2001
Online at stacks.iop.org/PPCF/43/A349

Abstract

Hydrogen isotopes are released from the walls, divertor plates and limiters of fusion devices in different forms, as atoms or molecules. The density and velocity distributions of these particles upon release can heavily influence the boundary plasma, especially through their penetration depth, and, indirectly, the plasma and its confinement properties as a whole. Recent experiments on different tokamaks have brought to light the deep interdependence between atomic and molecular species in this respect. Investigating this complexity calls for sophisticated spectroscopic diagnostics and new data on molecules like D_2 and HD. Hydrogen and deuterium atoms with extremely low energies, definitely below 1 eV, are observed and give indications on the release processes, i.e. on those where molecules are involved. It turns out that corrections to the estimated hydrogen flux may be required—a procedure is proposed in the present work to obtain values for an effective *S/XB* coefficient for atomic hydrogen ($\neq 15$), which denotes the ratio of the collisional ionization (S) to the excitation (X) rate coefficients, divided by the branching ratio B. Moreover, attention is drawn to a possible heating mechanism of these very cold atoms by the proton/deuteron background (from 0.2 up to 10 eV). The derived information on the detailed release mechanisms should contribute towards improving the various numerical codes in which neutrals play a role. Eventually, the strong influence of the surface temperature on the ratio of atoms to molecules has to be considered in the choice of materials for plasma-facing components.

1. Introduction

Although hydrogen isotopes are the fuel of current and future thermonuclear fusion devices, still too little is known at present of the detailed recycling processes which actually take place in the edge of magnetic fusion plasmas. Yet, this knowledge remains a matter of prime importance for the choice of plasma-facing materials and for their design parameters. Hydrogen, deuterium and, in future, tritium [1] are released in either atomic or molecular form, and in any of the possible isotopic combinations. The interplay between these different species, especially in the simultaneous presence of atoms and molecules, is increasingly becoming the subject of elaborate studies. Even at low to moderate kinetic energies, the corresponding high velocity of these lightest elements may lead to considerable penetration depths. Hydrocarbon molecules play a very important role too, especially in divertor environments, and deserve their own, detailed investigations [2–5]. The present paper concentrates on atomic and molecular hydrogen. The question of long-term behaviour, especially of overall particle balance and hydrogen retention, is also discussed elsewhere [6–8].

The definite influence of the processes involving both hydrogen atoms and molecules on fuelling and confinement properties is indisputable. This discovery may be illustrated by, among others, recent indications that the neutral pressure in the plasma boundary determines the quality of confinement in a certain class of radiatively improved modes of operation: strong gas fuelling readily leads to confinement degradation, even though the injected flux remains low with respect to the total recycling flux re-entering the plasma of TEXTOR [9–11]. High performance at trans-Greenwald densities thus depends on moderate gas inlet rates, possibly even on the total amount of hydrogen let in. Similar findings regarding the influence of the edge neutral properties on the core confinement were made on other tokamaks, like TFTR [12], D III-D [13] and ASDEX [14].

In most cases, though, the larger fraction of the particles needed to fuel the plasma enters through recycling processes [15] and one could state that 'the wall determines the plasma'. The external fuelling generally represents a small perturbation, the significance of which depends on specific conditions of the global plasma. This is another strong motivation for studying the implications of recycling.

One of the main goals of the current investigations is the identification of the physical release mechanisms from plasma-facing components (PFCs). An exhaustive list of the possible processes is beyond the scope of the present paper. Early reviews had identified the most important ones, albeit not with the detail attained in recent years [16, 17]. Let us mention for instance the following, some of which will be considered here: reflection, physical sputtering (of hydrides or hydrogen-saturated metals), ion-induced desorption of atoms, molecule release through thermal or prompt desorption, following the so-called Langmuir–Hinshelwood recombination, or an Eley–Rideal reaction (cf figure 1, [18]). Note that, of these processes, all but the first one lead to low energies of the released particles, in the eV range. One has to bear in mind that exposed surfaces are subject to continuous bombardment by ions and fast charge-exchange neutrals with energies in the 100 eV range, the fluxes and actual energy distribution of which are largely unknown through lack of diagnostics (one notable exception being perhaps time-of-flight spectrometry [19, 20]).

As the major component of fusion plasmas, hydrogen has been subjected to the most intensive and lengthy spectroscopic studies, most of which duly take advantage of the accessibility of its strong spectral lines in the visible range (Balmer series, transitions α to δ from 656 nm down to 410 nm). The main resonance line, Lyman-α at 121.5 nm, belongs to the vacuum–ultraviolet spectral range (VUV) and is accordingly much more difficult to observe [21, 22]. Yet its attractiveness still lies in its connection to the atomic ground state.

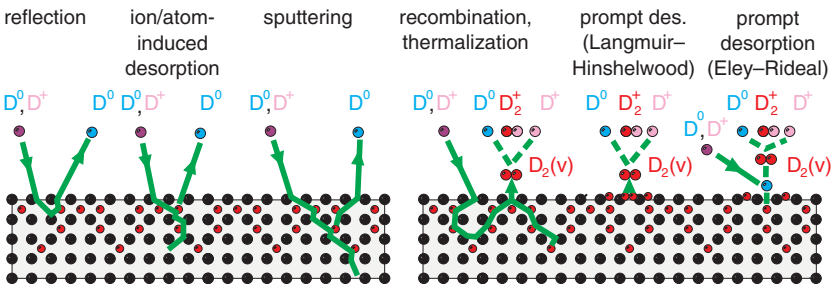

Figure 1. Different release mechanisms of hydrogen from plasma-facing components.

Admittedly, the Lyman series of hydrogen exhibits quite easily a noticeable opacity for the tokamak-relevant measurements, a situation which has to be taken into account [23, 24]. The spectroscopic investigations give clues to the hydrogen release from wall, limiters and divertor elements, and, as will be shown below, are best when both atomic and molecular aspects, low and high resolving powers, and even visible and ultraviolet spectral ranges are combined. Local densities, velocity distributions and fluxes are the quantities which call for experimental, *in situ* determination.

2. Available diagnostics and correlated quantities

2.1. Emission spectroscopy

The description of the experimental set-up for emission spectroscopy on TEXTOR (see figure 2) will serve here as a guide for the discussion. These systems can rely on good accessibility to the scrape-off layer and, from the last closed flux surface (LCFS) into the plasma, as deep as $r/a = 0.85$. Another interesting feature is the presence of high-resolution spectrometers, but other tokamaks certainly do not lag behind, as will be clear in section 3, when we discuss specific results from Tore-Supra, Alcator C-Mod, Asdex Upgrade in the divertor region or even from the main chamber of a larger machine like JET. Figure 2 shows the arrangement in the sector of one of the vacuum locks, which is used to bring test limiters and other PFCs from the bottom into the torus. Two ports are directed towards the observation volume in front of the inserted components. One line of sight looks at the limiter head from the top, the other one tangentially from the side, in the poloidal direction.

Both directions of observation can be equipped according to the needs for atomic spectroscopy with diffraction grating spectrometers in the Balmer range, attaining resolving powers $\lambda/\Delta\lambda$ up to $R \geqslant 90\,000$ ($\Delta\lambda \leqslant 8$ pm, D_α observed in the diffraction order $m = 37$ with an echelle grating, used for the determination of the atomic temperatures or, alternatively, to record velocity distributions of the flux perpendicularly to the limiter surface [25, 26]). To cover the somewhat broader range of the molecular Fulcher band, a dedicated spectrometer with $R \cong 13\,000$ ($\Delta\lambda = 50$ pm) is used between 600 and 640 nm for flux determination and with the goal of assigning rotational and vibrational temperatures to the observed isotopomers. Additional devices include a two-dimensional camera with a 10 nm wide interference filter for the determination of the flux at the same location, i.e. on the very same limiter head, and an additional spectrometer ($R > 8000$, $\Delta\lambda = 50$ pm around D_γ) at the tangential port to record penetration depths with a resolution of 0.5 mm.

Note that the vacuum lock is quite flexible and allows insertion of various limiter heads and other plasma-facing components, with active heating and bulk temperature stabilization

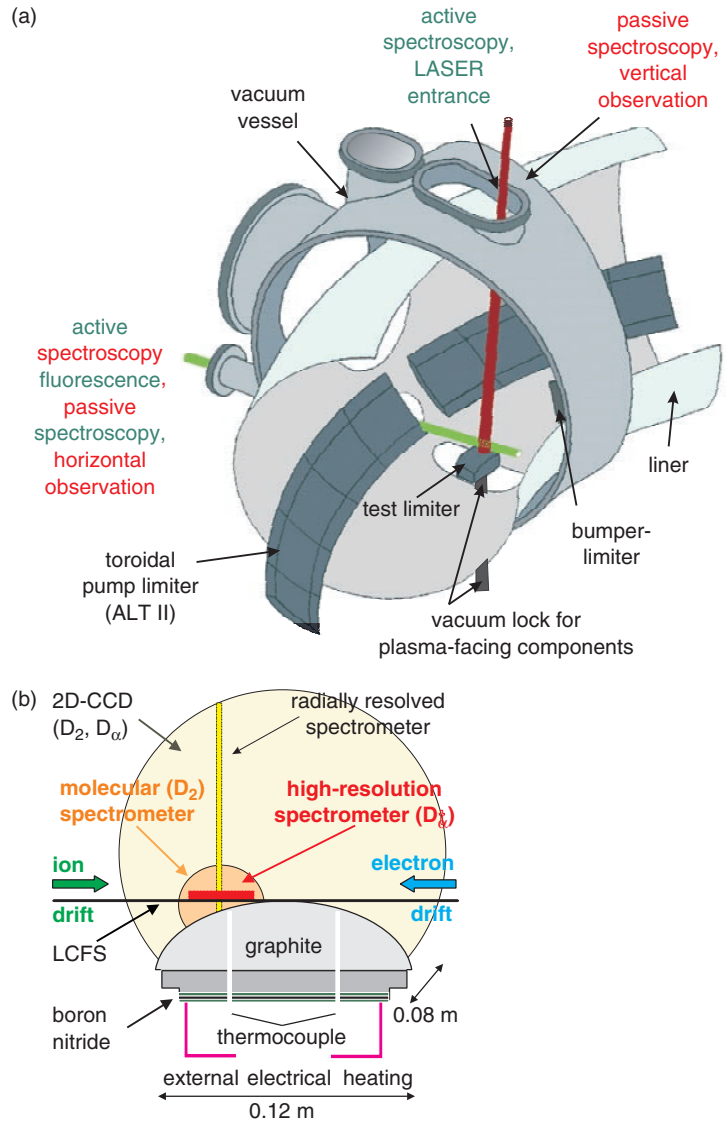

Figure 2. (*a*) Experimental set-up for active and passive spectroscopy in the limiter-lock section of TEXTOR. (*b*) Geometry of the spectrometers' observation in front of a limiter head (side view through horizontal port).

up to a homogeneous $T = 1500\,\mathrm{K}$ or with holes for gas injection, or even, for calibration purposes, heated gas inlet nozzles at pre-set radial positions.

Other important directions of observation away from the vacuum lock include a toroidal view of the main poloidal limiters in the upper part of another section, head-on views at some locations of belt-limiter blades (flux measurements on Advanced Limiter Test II (ALT II)) and toroidal observation of the edge plasma along the magnetic field lines [27], thus eliminating the π-components of the Zeeman pattern ($R \cong 40\,000$ at D_α).

2.2. Active diagnostics

2.2.1. Laser-induced fluorescence The upper port in the set-up (see figure 2) is also used as an injection window for the L_α beam of the laser-induced fluorescence (LIF) system at 121.5 nm. It is used to measure the velocity distribution and density of atomic deuterium in the ground state, within a small fluorescence volume of about 0.5 cm^3 (0.3 cm radial extension × 1.5 cm beam diameter). The velocity is measured in the vertical, i.e. radial, direction of the laser beam according to figure 3(*a*). The observed volume is imaged onto a gated, solar-blind photomultiplier by means of an achromatic Cassegrainian telescope which can be tilted up and down. By controlled elevation, it is thus possible to move the observation volume radially along the laser beam to obtain radial profiles as well. The VUV laser system is described elsewhere [28]; its recent, improved version is based as before on a powerful excimer-pumped dye laser [29], the near-ultraviolet output of which is converted to L_α by frequency tripling in a noble gas cell [30, 31]. The repetition rate has been increased from 20 to 50 Hz for better statistics and the spectral width of the laser reduced, thanks to a double-grating arrangement,

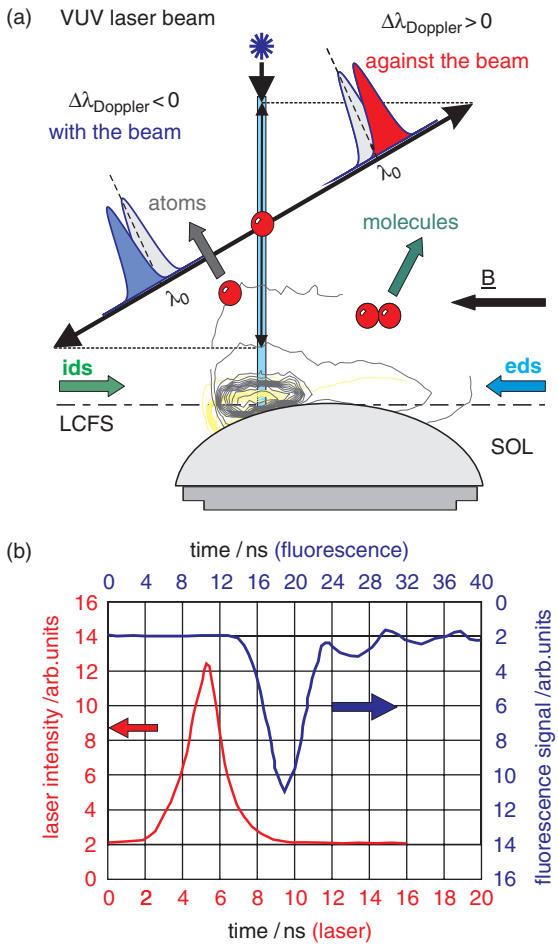

Figure 3. (*a*) Geometry of the experimental set-up for LIF in front of a limiter head. (*b*) Time traces of a vacuum–UV laser pulse and of the corresponding fluorescence signal at Lyman-α.

to $\Delta\lambda_{\mathrm{LAS}} \cong 0.6$ pm in the VUV, or $R \geqslant 200\,000$ without the need for inserting and adjusting any additional intra-cavity Fabry–Pérot étalon. Figure 3(*b*) shows time traces of the VUV laser pulse and of the fluorescence signal in the centre of the line [32].

2.2.2. Further active diagnostics: thermal atomic beams Apart from the limiter lock system and its active heads, described in section 2.1, the evaluation of the spectroscopic data is supported by diverse atomic beams, which provide the electron density and temperature (n_{e}, T_{e}) at various toroidal and poloidal positions in the boundary layer. A thermal lithium beam is installed in the outer equatorial plane for the continuous measurement of n_{e} profiles in the plasma edge (observation of the Li I-resonance line at 670.8 nm). Four different collimated helium beams (top, bottom, low- and high-field sides) give n_{e}, T_{e} from line intensity ratios between singlet, or singlet to triplet transitions, with high temporal and spatial resolution, i.e. below 1 ms and 1 mm, respectively. We refer to the literature for details on the spatial, density and temperature ranges covered [33, 34], which correspond roughly to $r/a = 0.85$–1.2, $n_{\mathrm{e}} = 1.0 \times 10^{18}$ to $2.0 \times 10^{19}\,\mathrm{m}^{-3}$ and $kT_{\mathrm{e}} = 10$–200 eV.

3. Atoms or molecules?

The omnipresence of molecules in the edge plasmas of magnetic fusion devices was recognized recently. They were naturally taken into account in the dense and cold—some processes appear below 3 eV—divertor region of corresponding configurations. It took longer to recognize them more universally in boundary plasmas, partly under the impulse of the findings of atomic spectroscopy. The specific role of molecules in a divertor plasma and their influence on the recombination processes, in particular on the so-called 'molecular assisted recombination' (MAR [35, 36]), is discussed extensively in [37] for a specific case. Discussions on the divertor case and its specific dynamics can be found in the literature [37, 38].

3.1. Atomic spectroscopy and the occurrence of 'cold' atoms

First indications of a broad range of low atomic energies were reported early by Bogen *et al* [39, 40], with emission spectroscopy and laser fluorescence as well, and followed very soon with tentative explanations involving molecular dissociation processes, like electron impact dissociation or dissociative excitation, yielding a pair of free electrons with different energies (velocities v, v') [41, 42, 25]:

$$\mathrm{H_2} + \mathrm{e} \rightarrow \mathrm{H^+} + \mathrm{H}(n = 3) + \mathrm{e}(v) + \mathrm{e}(v').$$

Two complementary (synallagmatic) measurements covering the same plasma radii were performed on TEXTOR, mutually confirming the substantial number of slow deuterium atoms in the velocity distributions, consistently with the possible molecular origin of the atoms responsible for the line core. On the one hand, a sophisticated evaluation by Hey *et al* [27] of the spectral line shape of Doppler-broadened Balmer α–γ profiles recorded along the magnetic field lines in the edge ($r/a = 0.95$–1.1) revealed the presence of at least three components in the atomic temperature; the coldest one, corresponding to energies in the range $kT_{\mathrm{cold}} = 0.3$–0.5 eV, appears for all heating conditions or radial positions within the mentioned limits in the plasma discharges which were investigated. A typical example of a spectrum obtained by observation nearly tangentially to the magnetic flux surfaces is shown in figure 4. This displays profound dips at the position of the missing π between the σ-components of the Zeeman pattern, in a now familiar picture for different fusion devices. A later, refined

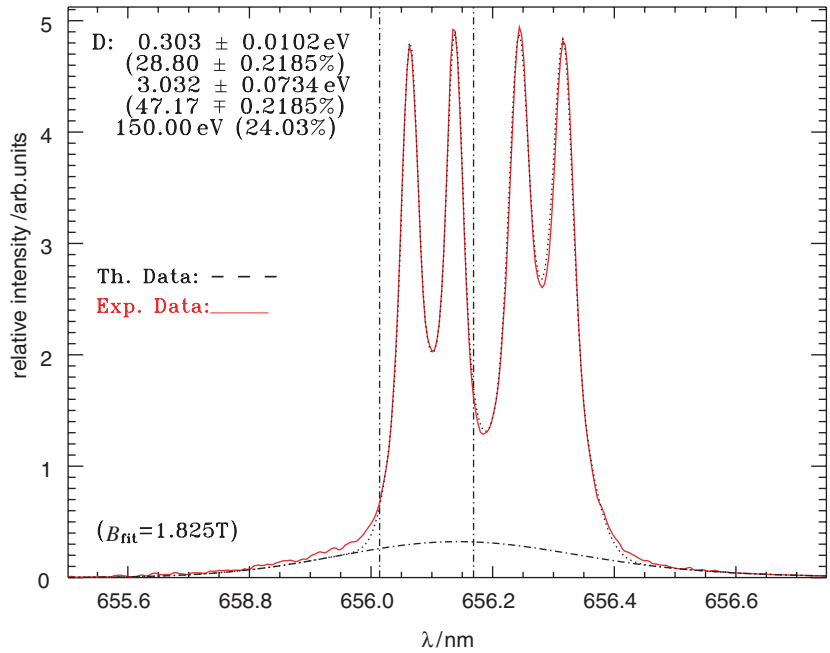

Figure 4. Spectral profile of the Balmer-α line in an NBI-heated discharge (1.1. MW, TEXTOR 70860) at $r/a = 0.95$. Profile analysis yields three atomic temperature classes (given in eV) whose origins and relative proportions are discussed in [43, 79].

analysis of similar profiles recorded with different isotopic ratios, which takes into account the analytical model discussed in section 4.2, is given in [43].

On the other hand, LIF measurements by Mertens [44, 28] in the vicinity of the wall, at $r/a = 0.96$–1.2 as above, brought to light somewhat unexpected velocity distributions for the ground state of deuterium: the largest contribution to the density in the spectral profiles recorded up to the equivalent of 20 eV definitely lies below 4 pm, i.e. below a kinetic energy of 1 eV ($\bar{v} < 1.0 \times 10^4$ m s^{-1}) in the radial direction of propagation, perpendicular to the magnetic field. The peak may lie as low as 0.20–0.30 eV. This even holds true in front of plasma-facing elements, e.g. the graphite surface of a test limiter, as deeply as 10–20 mm inside the LCFS depending on the type of discharge, in full agreement with the previous findings. Figure 5 shows recent distributions where the structure of the fluorescence signal depends on the toroidal position of the observation volume, i.e. on the distance to the spot which is exposed to the main plasma load.

In emission spectroscopy, the occurrence of these particular velocity distributions was assigned to molecular reactions of the type [27, 43, 44]

$$\mathrm{H_2 + e \rightarrow H_2^{**} + e}, \qquad \mathrm{H_2^{**} \rightarrow H^*}\ (n = 3, 4, 5) + \mathrm{H}(n'\ell) \qquad \text{with } n' \geqslant 1,$$

or alike, involving the dissociation of the molecular ion. It should be stressed that these low energies are not only found in the high-density region of a divertor [37] or MARFEs [45] but, in this case, in the plasma edge of a limiter tokamak ($kT_e \approx 20$–120 eV), the central electron temperature of which may be higher than 2 keV.

Departing from the usual assumption of Franck–Condon energies around 2 eV for the atomic products of molecular dissociation [46], it is clear with these results that processes with output energies as low as 0.2 eV have to be taken into account. Such assumptions are in

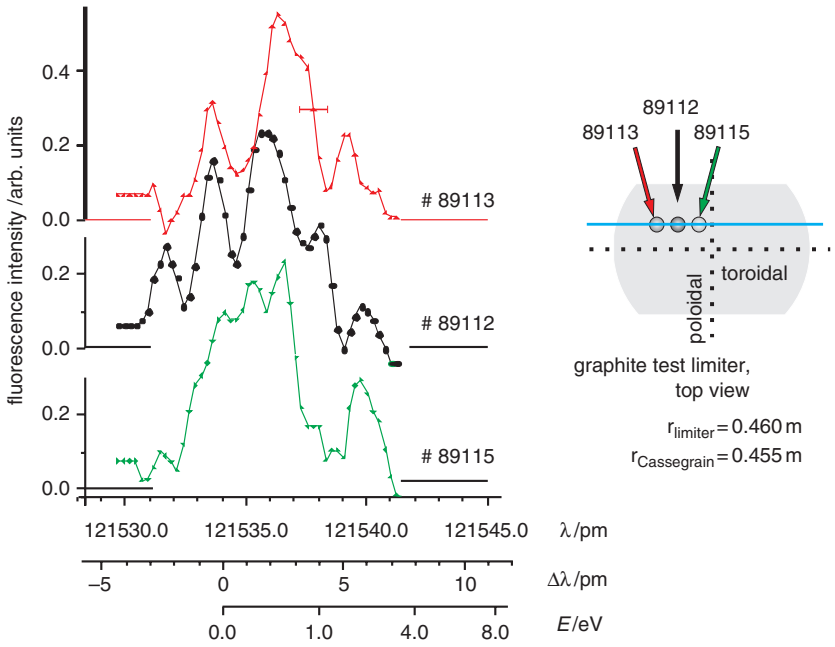

Figure 5. Velocity distributions of atomic deuterium in the ground state, in front of a graphite limiter. The spectral profiles are recorded by means of LIF at Lyman-α (the laser beam is driven back and forth in the toroidal direction) [32].

agreement with other measurements on different tokamaks, from the low-T_e case, for instance in HT-6M ($\approx$ 10 eV at the limiter [47]) or in the divertor region of JT-60U [48], to the higher T_e values of the three following examples.

A spectral emission profile of atomic deuterium, taken about 10 mm in front of an equatorial neutralizer plate of the ergodic divertor in Tore-Supra, is shown in figure 6(*a*). The He II Brackett line, the position of which is indicated by the broken vertical mark, does not disturb the deuterium spectrum for the given conditions [49, 50]. The temperature which was assigned to these profiles ranges from $kT_{D0} = 1.4$ to 2.5 eV depending on the local plasma parameters, especially on the electron density n_e at the edge [51]. Details on the evaluation of similar spectra are given in [52] for asymmetric profiles recorded at the same location; the concentration of atomic hydrogen is generally too low to be considered in these shots. The measurements were indeed followed by an evaluation of the molecular contribution to the flux [53].

The temperature of atoms was also investigated by Welch in the edge region of Alcator C-Mod [54, 55] during both limited and diverted discharges. Figure 6(*b*) gives an example of these. The lowest temperature of $kT_{D0} = 0.86$ eV arises from within the divertor, but the otherwise recorded values of 2.1–3.8 eV, although seemingly in better agreement with the Franck–Condon range, actually correspond to much lower temperatures after correction for other broadening effects. The asymmetries due to different emitting regions of the plasma are taken into account.

In spite of the different conditions, there are striking similarities in the Balmer-α profiles recorded by Mertens near the wall of JET's main chamber with the high-resolution spectrometer of the 50 kV lithium beam, diverted in this instance from its primary use ($R > 8000$, $\Delta\lambda = 80$ pm around D_α [56]). Due to the periscope arrangement [57], many

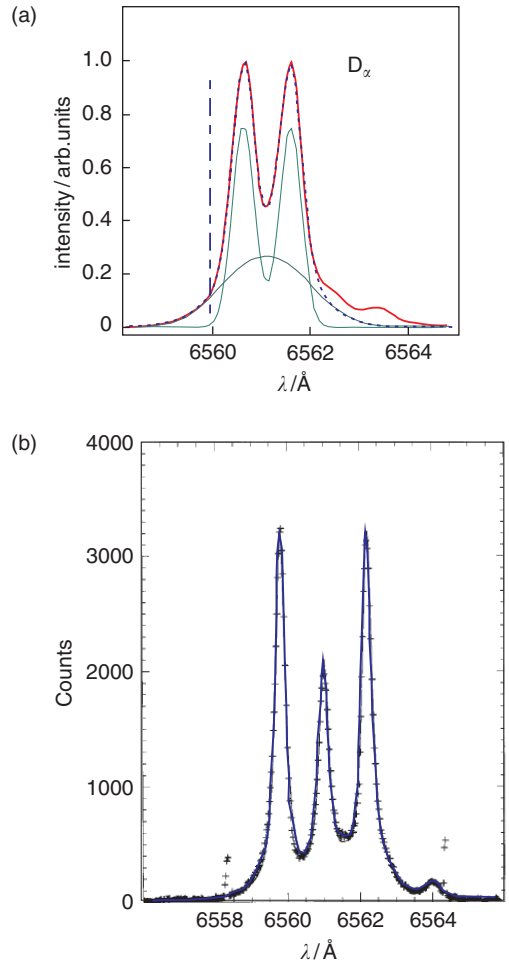

Figure 6. Spectral profiles in the Balmer-α region recorded in different tokamaks (**I**): (*a*) Tore-Supra in front of a neutralizer plate, (*b*) Alcator C-Mod (see text, and [55] for explanations).

lines of sight cross the layer of atomic hydrogen and deuterium at the wall under observation angles which are close to the direction of the magnetic field. Figure 7(*a*) gives an impression of their geometry [58], where the curved lines account for the descending viewing lines along the toroidal direction, folded back into the plane of the drawing. Accurate evaluation will therefore rely, on the one hand, on the knowledge of the local field strength, to be correlated with the Zeeman splitting, eventually requiring equilibrium reconstruction for specific points in time. On the other hand, it will also be based on the assumption that three temperatures contribute to the Doppler broadening, as was realized in the first fitting attempts. The preliminary value for the atomic energy, below 1 eV, more precisely $kT_{\mathrm{cold}} < 0.6\,\mathrm{eV}$ (figure 7(*b*)), may nevertheless be considered again as surprisingly low, in view of the otherwise high temperatures reached in such large plasmas.

Although the present, direct juxtaposition as above of results gathered in different plasma edge regions of various tokamaks is an extremely crude presentation, not doing justice to the detailed analysis of each specific case, these accurate measurements on the atomic hydrogen

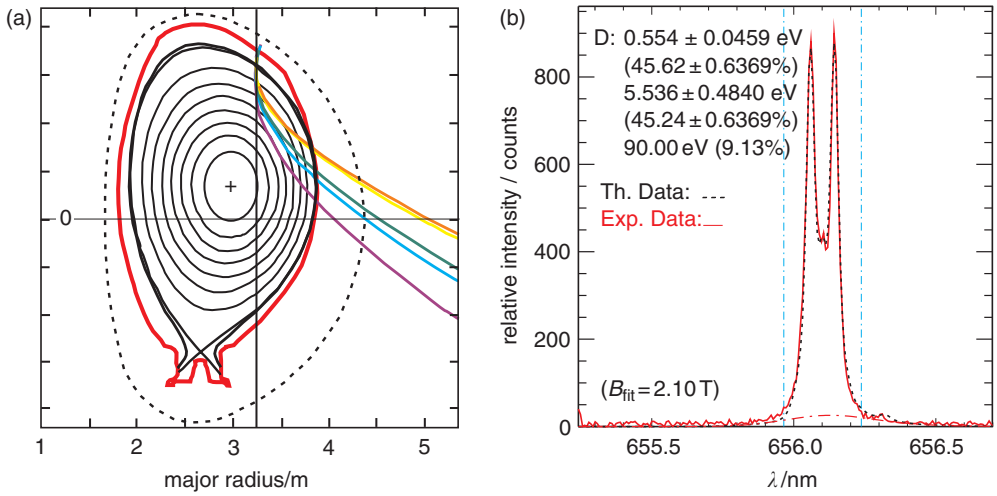

Figure 7. Spectral profiles in the Balmer-α region recorded in different tokamaks (continued): JET in the vicinity of the wall (main chamber). (*a*) Lines of sight, (*b*) spectral profile (JP52642L).

isotopes increasingly give indications that more molecular processes are involved than expected before, and that a broad range of temperatures can be found, even if one considers the so-called 'cold' components only, which range from about 0.2 to 2.5 eV at most. A sustained effort in the field of molecular spectroscopy was therefore required in order to explain these phenomena. Some of the recent results are discussed in the following section. This comes in addition to the work to which Stangeby [59] pays tribute, mentioning molecular mechanisms in relation to their actual relevance to plasma–surface interactions.

3.2. Molecular spectroscopy

For the following discussion, one should keep in mind the level diagram for molecular hydrogen or deuterium which is schematically drawn in figure 8, in an extremely simplified version (specifically valid for D). The ground state—inaccessible to our passive spectroscopy in the tokamak—belongs to the singlet system, whereas the strongest detectable radiation corresponds to transitions between excited triplet states. Each electronic level splits, as detailed for the ground state only, into vibrational sublevels (with index v, . . .) which, in turn, correspond to rotational sublevels, the discussion of which is beyond the scope of this work.

3.2.1. Observation of the Fulcher band of H_2 and D_2 First quantitative measurements on H_2 molecules were performed on TEXTOR [60]. It turned out that the intense Fulcher transition ($d\,^3\Pi_u - a\,^3\Sigma_g^+$), in the visible range from 600 to 640 nm, is among the most suitable ones to provide information on molecular hydrogen and deuterium, owing to its accessibility and the fact that it is free of overlapping with other bands and therefore can be interpreted more reliably. It gives access to the vibrational and rotational populations in an excited state, which have to be mapped, through Franck–Condon factors, down to the ground state with techniques proposed i.a. by Fantz and Heger [61] and applied successfully to the divertor region of ASDEX Upgrade [62] (see figure 9). If the excited states are populated by processes other than electron impact from the ground state and loss mechanisms other than radiative decay are involved, it is obvious that a collisional-radiative model is required (see section 4.3).

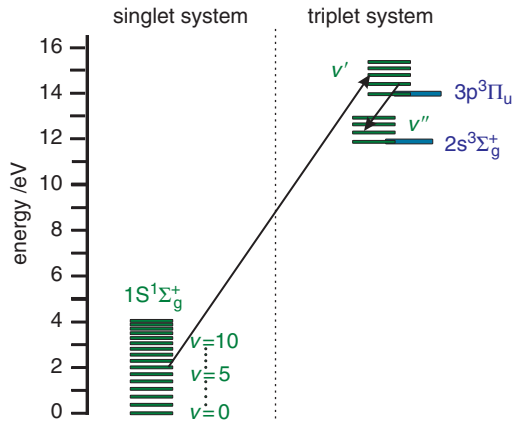

Figure 8. Excerpt from a Grotrian diagram for the deuterium molecule. Displayed are only the energy levels relevant to the following discussion. The levels are slightly displaced with respect to the case of hydrogen and present a different distribution of the vibrational sublevels.

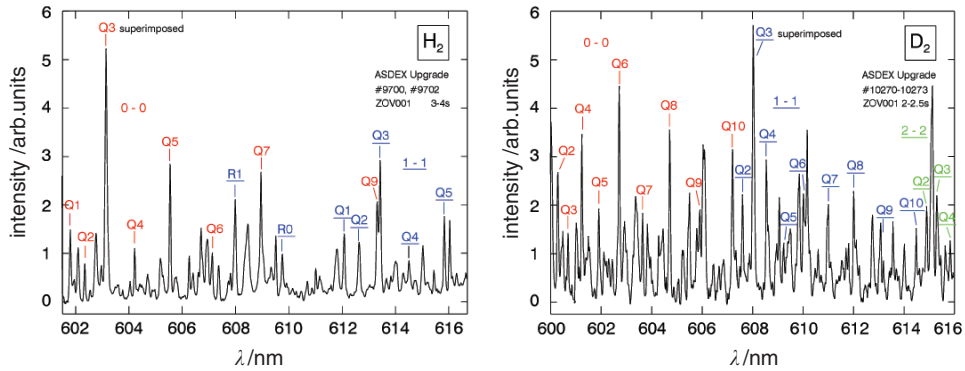

Figure 9. Hydrogen and deuterium molecular spectra recorded in the divertor region of ASDEX Upgrade (U Fantz).

3.2.2. From H_2 to D_2 and HD The interplay between hydrogenic atoms and molecules also takes place within the edge plasma of TEXTOR, in front of graphite surfaces. Concurrently to the extension of the above-mentioned techniques from hydrogen to deuterium molecules, spectra were recorded *in situ* by Brezinsek which display in a demonstrative way all three isotopic combinations H_2, D_2 and HD (figure 10), the main diagonal ($\nu'' = \nu'$) transitions of which are identified in the picture. Wavelengths for the deuterium molecules, from the work of Dieke and co-workers, can be found in Freund *et al* [64]. The results of the following section were obtained through measurements on molecular deuterium. Molecular data for correct quantitative evaluation of such spectra are still partly lacking, in increasing order of need for D_2 and HD molecules. Discrimination between the three isotopic combinations is nevertheless possible and of great use, provided a sufficiently high resolving power is available.

3.2.3. Influence of the surface temperature, T_{surf}, on the release processes In order to provide a clear separation between the different release mechanisms, laboratory measurements were performed by Franzen and Vietzke [65]. They have demonstrated that driving the temperature

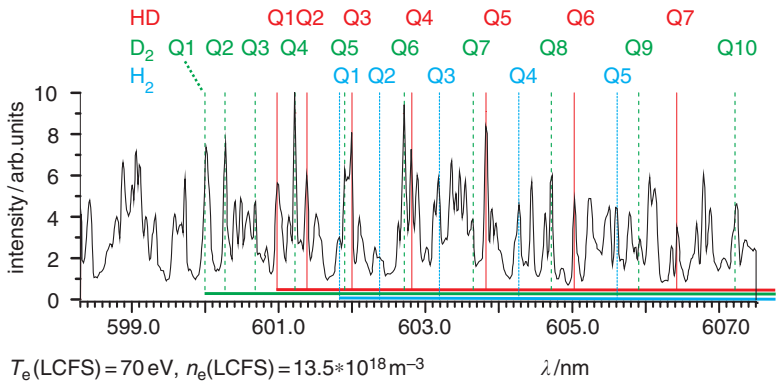

Figure 10. Molecular spectrum recorded in front of a graphite surface in TEXTOR. Ro-vibrational transitions of H_2, D_2 and HD are identified [63] in terms of the relevant Q-branches, corresponding to $\Delta J = 0$, and to the vibrational transitions $v' = v'' = 0$.

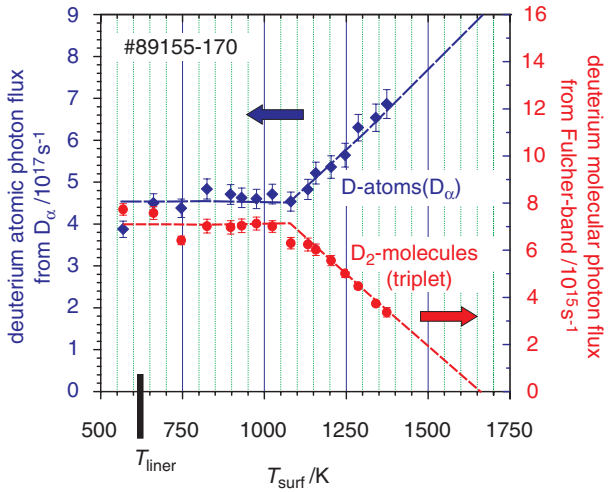

Figure 11. Variation of the photon fluxes emitted by the atoms (upper trace) and molecules (lower trace) in front of a heated limiter versus surface temperature (*in situ* measurement) [63].

of a graphitic surface, from which hydrogen is released, is one controlled way of modifying the ratio of atomic to molecular fluxes which are thermally desorbed or re-emitted from graphite. Owing to its relevance as a material for plasma-facing components, graphite naturally came in the first place in our investigations. In a way similar to the laboratory experiments, the method was applied *in situ* on an active limiter, heated up and stabilized, with results in full agreement with the previous findings [66, 63]: as shown in figure 11, atomic and molecular photon fluxes in front of the graphite surface display a sharp bend around $T_{\mathrm{surf}} = 1100\,\mathrm{K}$, which corresponds to a pronounced increase in the atomic flux, for both D_α and D_γ, and an equally pronounced decrease of the molecular contribution. In the evaluation of the latter, a large number of rotational components of the diagonal band (Fulcher-α) were taken into account, namely Q1–Q8, so that the temperature at which the clear transition occurs can be pinpointed with confidence [66]. Thanks to an absolute calibration, extended through a cross-calibration with injection of a known amount of gas, both curves provide actual

photon fluxes Φ^{D}_{phot} and Φ^{D2}_{phot}. At the extrapolated temperature $T_{surf} = 1700\,K$, molecules would really vanish. Similar measurements on H^0 instead of D^0, but resorting to the H_δ line for the atoms and to another molecular band in the singlet system around 430 nm for $H_2(3d\,^1\Pi_g \rightarrow 2p\,^1\Sigma_u^+)$, lead to identical conclusions with respect to a sharp transition against T_{surf} [66]. This agreement between measurements on different isotopes, which even rely on different optical transitions, gives indeed a strong confirmation of the dependence of the flux ratio on the surface temperature.

The question arises as to whether such quantities as a rotational or a vibrational temperature, T_{rot}, and T_{vib}, make any sense under such conditions. For the rotational temperature of the upper state observed, the answer is positive. It could be checked for the first eight rotational lines from each vibrational level. This T_{rot} increases monotonically with T_{surf} and with the electron pressure; the most obvious explicit dependence seems to be on $n_e|_{LCFS}$ in front of a limiter [67]. It might even be used as an indirect means of monitoring this or other plasma parameters. Noteworthy is the population distribution in the ground-state vibrational levels, which can be derived from five to six vibrational states of the diagonal Fulcher band along the lines discussed in section 3.2.1: what emerges is an overpopulation of $v' = 3$ for the recycling at plasma-facing components made of graphite. No real T_{vib} can therefore be assigned to the molecular deuterium—a surprising result at first glance, but in accord with known distributions bound to the release of molecules from graphite or metallic surfaces [18, 68]; the corresponding desorption processes, named Eley–Rideal or Langmuir–Hinshelwood, are mentioned in our introduction. A vibrational temperature therefore corresponds to the few states which align on a Boltzmann distribution. The deviation of $v' = 3$ is shown in figure 12, mapped to the upper states. This not only looks like a serious clue to the presence of molecules and the possibility to measure their spectra routinely in a tokamak, but it also gives clear access

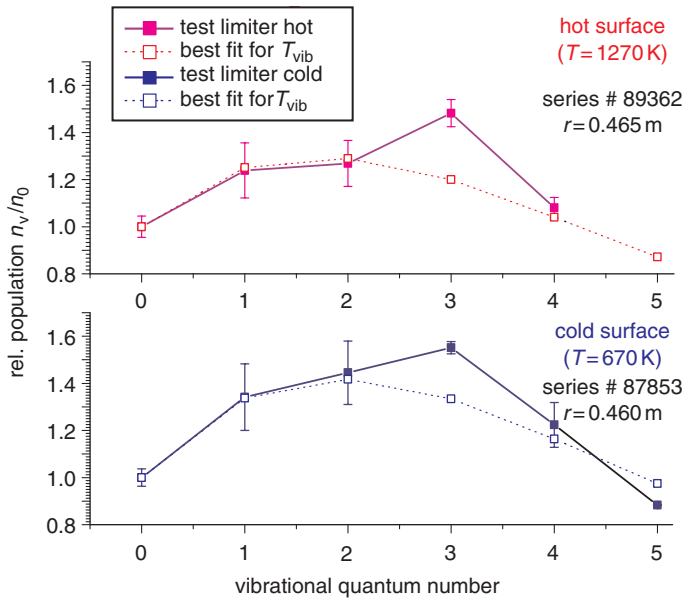

Figure 12. Vibrational distribution—in the upper state—of molecules released from a hot or a cold limiter surface in TEXTOR under similar plasma conditions. The dotted profiles represent the distributions derived from $T_{vib} = 3730\,K$ ($\pm 400\,K$) and $T_{vib} = 3370\,K$ ($\pm 400\,K$), respectively, in the ground state.

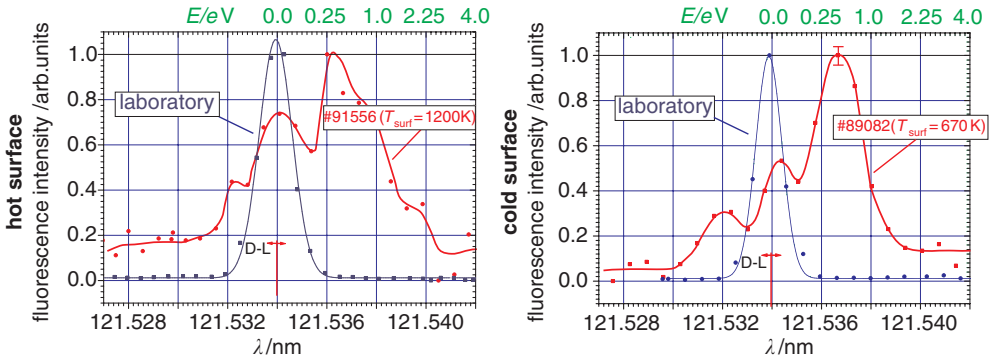

Figure 13. Velocity distributions of atomic deuterium released from a cold and a hot limiter surface (LIF). In both cases, $n_e \approx 2 \times 10^{18}$ m^{-3} and $T_e \approx 80$ eV, $r_{lim} = 46$ cm (LCFS), distance to surface-9 mm.

from the molecular ground state to dissociation processes through higher, electronically excited repulsive states, which lead through dissociative excitation to products—the atoms—with very low energies.

One should bear in mind that the rotational temperature depends upon, and thus gives an indication of, the electron density. In a similar way, the vibrational temperature, if one can be assigned, may be used to monitor the electron temperature, at least for the divertor case [69].

Closely connected to the local heating of the surface of plasma-facing components, a simultaneous LIF measurement of the atomic velocity distributions is shown in figure 13 for both cases as before [70]. These distributions display a pronounced increase of very cold atoms for higher T_{surf}: as a matter of fact, much higher temperatures lead to even colder atoms, which points to still other release mechanisms, in agreement with the finding that the ratio of atoms to molecules then tends to infinity, as previously confirmed (cf figure 11 and related discussion). It means that the molecular flux becomes negligible and that atoms are released with temperatures tending to the surface temperature.

3.3. Photon fluxes and particle fluxes

The main purpose of emission spectroscopy in the visible, applied in the present case to atomic hydrogen, is the determination of the particle flux. The influx of neutrals is proportional to the ionization rate, under the assumption of negligible recombination. Since ionization and emission of Balmer lines take place concurrently, the following most widely used formula is applicable and gives the particle flux (number/s) [71, 60]:

$$\Gamma_0 = 4\pi \frac{I_0}{h\nu} \frac{\int_{r_1}^{r_2} n_0(r)\, n_e(r) \langle \sigma_i v_e \rangle \, dr}{B \int_{r_1}^{r_2} n_0(r)\, n_e(r) \langle \sigma_{ex} v_e \rangle \, dr}$$
$$= 4\pi \frac{I_0}{h\nu} \frac{S}{XB},$$

with the measured intensity I_0, neutral and electron densities $n_0(r)$ and $n_e(r)$, the rate coefficients $\langle \sigma v \rangle$ for ionization and electron impact excitation respectively, and the corresponding branching ratio B. The other symbols bear their usual meaning. Integration takes place over the whole attenuation length.

The quantity S/XB, which denotes the ratio of the collisional ionization (S) to the excitation (X) rate coefficients, divided by the branching ratio B, is accordingly of prime

importance for flux measurements. The commonly accepted value of about 15 for D_α, for instance, taken in a wide range of electron temperatures (the most sensitive factor) around 20–200 eV may have to be corrected to account for the presence of molecules. The need for such a correction will, of course, arise *a fortiori* in the occurrence of lower electron temperatures. It should be stressed that the hydrogen fluxes are given in number of particles, i.e. *atoms*, per second (and unit area for flux densities) whether molecules are present or not, that is molecules count twice since they contribute to two atoms.

Brezinsek *et al* [63] evaluates the corresponding factor D/XB for molecules, where the 'D' (for decay) stands for all loss mechanisms which accompany the spontaneous emission, and defines an effective $(S/XB)_{\mathrm{eff}}$, which allows for the molecular flux. Other authors (see e.g. Wünderlich [72]) use a similar procedure with slightly different notations. The main difficulty obviously lies in the determination of D/XB for the relevant plasma parameters (n_e, T_e). One has to resort to the balanced use of measurements of molecular spectra together with consistent collisional-radiative modelling (section 4). Figure 14(*a*) shows the D/XB factor for correction of the molecular contribution to the flux as a function of the local electron density and temperature, as obtained from a computation with the so-called 'CRMOL' code [73].

This factor is included in the evaluation which shows the photon flux from D_α versus the calibrated molecular flux (figure 14(*b*)). The intersection of the straight line with the ordinate obviously corresponds to the situation where 15 is the right value for S/XB (no molecules). The left-hand scale gives for this single point the absolute atomic flux of 3.1×10^{19} particles per second. If a molecular flux is present, the relevant D/XB factor applies to the conversion of the Balmer photon flux into a total deuterium flux through an effective $(S/XB)_{\mathrm{eff}}$ which sums up both contributions, atomic and molecular. In the present case, the applicable D/XB amounts to about 2000; this value is valid only for the prevailing electron density and temperature of $n_e = 5.5 \times 10^{18}$ m^{-3} and $T_e = 40$ eV, but the procedure can be applied for any conditions provided that an adequate, calibrated spectrum is available for the molecules.

More precisely, the conversion of Balmer-α photons to a hydrogen or deuterium flux is performed with the effective value:

$$(S/XB)_{\mathrm{eff}} = S/XB\left(1 + \frac{2\eta\Gamma_{\mathrm{D2}}}{\Gamma^{\mathrm{tot}}}\right),$$

where $S/XB = 15$, as commonly accepted in the 20–200 eV range [60, 71], η accounts for the number of emitted Balmer-α photons per molecule, which involves the type of dissociation process ($\eta = 1$ in the present case for dissociative excitation with the products $D^0(n = 3) + D^0(1s)$), Γ_{D2} is the calibrated molecular flux (molecules per second), $\Gamma_{\mathrm{D2}} = f(D/XB(n_e, T_e))$, and Γ^{tot} represents the total, constant deuterium flux, $\Gamma^{\mathrm{tot}} = \Gamma_{\mathrm{D}} + 2\Gamma_{\mathrm{D2}}$.

The influence of different factors on the ratio of molecules to atoms ought to be emphasized. Although the role of the surface temperature has been stressed in the foregoing discussion, since it represents a convenient external control parameter, other less controllable parameters may be decisive in determining this flux ratio: especially important may be the plasma density, as discussed by Pospieszczyk *et al* in [66]. Moreover, the material is decisive in this respect: recent D_β observations indicate that the surface temperature is important for graphite and, for instance, tantalum but might be regarded as less relevant in the case of tungsten [74, 75].

To sum up, if the quantitative measurement of a suitable molecular band—and Fulcher-α may be one of these, although not terminating in the electronic ground state—is performed concurrently to the emission measurement of one of the Balmer lines, the simplest one being of course Balmer-α, it is possible to convert in a much more accurate way the photon fluxes into particle fluxes, i.e. atoms per second.

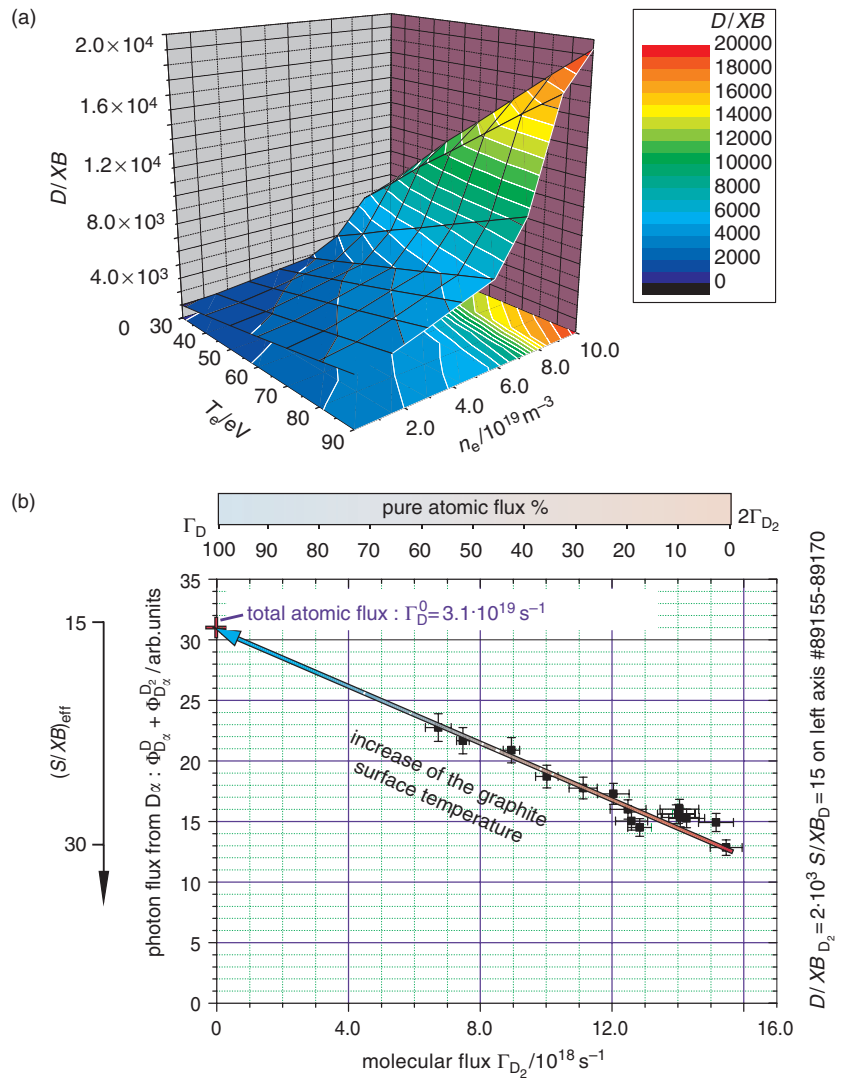

Figure 14. (*a*) *D/XB* factor for estimation of the molecular flux from the Fulcher emission. (*b*) Total flux estimated from the emission signal of Balmer-α [63]. The arbitrary units correspond, for TEXTOR, to an absolute value of $3.1 \times 10^{19}\ \mathrm{s}^{-1}$ in case no molecules are present (i.e. on the left axis). Again, the hydrogen flux unit is atoms per second, with molecules counting twice in the total flux: $\Gamma_D^{\mathrm{tot}} = \Gamma_D + 2\Gamma_{D2}$.

4. Analytical models and numerical codes

4.1. Paschen–Back effect and Zeeman pattern of the Balmer-series transitions

A rough criterion may be formulated for judging the importance of the Zeeman effect on spectral line profiles (transition $n \to n'$ in a hydrogenic atom or ion of mass μ in atomic mass units and ionization stage Z, with $Z = 1$ for neutrals), for relevant values of kT (eV) and

magnetic field strength B (T) [76, 77]. For temperatures less than

$$kT \leqslant \mu \left(\frac{n^4 B}{40 Z^2} \right)^2 ,$$

magnetic field effects may be expected to cause appreciable distortion of Doppler-broadened line profiles. For D_α, for example, with $kT = 1$ eV, a field strength as small as 0.3 T already causes a significant perturbation of the radiator fine-structure sublevels. Fields typical of the tokamak are indeed, therefore, so high, that it is essential to account for the Paschen–Back effect when attempting to extract Doppler temperatures from measured line profiles. This means, in particular, that the perturbing field is strong enough to induce the emission of Δj-forbidden components, and that the line strengths of individual Zeeman components differ significantly from their zero-field values. We proceed to outline the method of generating theoretical line profiles which can be used for spectroscopic analysis. Note that a useful table for the number of Zeeman components (allowed and forbidden) which participate in a transition between a given pair of principal quantum numbers is given in [76].

Unlike the case of multi-electron atoms and ions, the eigen-energies of the hydrogenic species are 'precisely' known, i.e. they may readily be computed to within the desired level of precision from known closed-form expressions, rather than taken from experimental data. In the absence of an external magnetic field, the eigen-energies are provided, firstly, by the solutions to the Dirac equation, corrected for nuclear motion. The leading quantum electrodynamic (QED) corrections ('Lamb shift contributions') to these eigen-energies are included only for the lowest values of the azimuthal quantum number ($l = 0, 1, 2$), being insignificant for the higher l-values [76]. The zero-field eigen-energies are now shifted in the presence of the magnetic field, with the consequent lifting of the m-degeneracy. The 'unperturbed' energies are obtained from the zero-field energies by adding to each the amount

$$\Delta E(n, l, j, m) = \mu_B g_j m B,$$

where g_j denotes the Landé g-factor and μ_B the Bohr magneton. Consistent with the precision to which the zero-field energies are evaluated, the expression for the Landé g-factors should include the effect of nuclear motion on the orbital gyromagnetic ratio as well as the two lowest-order QED corrections to the electron spin gyromagnetic ratio [27].

These 'unperturbed' energies in the presence of the magnetic field form the basis for the calculation of the perturbed (Paschen–Back) energies and line strengths by the process of solving for the eigenvalues and eigenstates of the appropriate tri-diagonal matrix, set up for each set of ($nlm \rightarrow nl'm'$) values, where m ranges from $-(l + 1/2)$ to $(l + 1/2)$, $l' = l \pm 1$, and $\Delta m = 0, \pm 1$, respectively, for the π and $\sigma_\pm$ spectral components. The diagonal elements of the matrix contain the 'unperturbed' magnetic sublevel energies, evaluated as outlined above, while the off-diagonal elements contain the Paschen–Back perturbation, which connects states of the same s-, l-, and m-value, but having j-values differing by one unit. This perturbation is thus absent in cases where m assumes its maximum (minimum) allowed value, and the corresponding line strengths remain unaltered for all B-field values. In associating the perturbed with the zero-field states, the no-crossing rule of von Neumann and Wigner must be strictly fulfilled. While the present computations follow a well-documented technique (e.g. Condon and Shortley [78]), they represent an important extension of the methods presented in the standard literature, since we account for the general case where *both* the upper and the lower terms of the transition are perturbed. We therefore allow in general for the existence of Δj-forbidden transitions, the theory of which has been much neglected since the earliest pioneering theoretical and experimental work. It is important to emphasize that the quantum-mechanical *phases*, which arise through the use of the square roots of the zero-field line strengths, rather than the line strengths themselves, must be meticulously observed.

4.2. From 0.2 to (1–10) eV*: a likely heating mechanism*

We pointed out above the presence of a substantial number of atoms with low kinetic energies around 0.2–0.3 eV, which are responsible for the occurrence of the coldest components in the Doppler-broadened profiles. Evaluation along the lines of the previous section suggests that they are produced by molecular dissociation upon electron impact as mentioned on several occasions, more precisely by dissociative excitation. However, whereas LIF observations in the plasma edge reveal a narrow range of kinetic energies along the laser beam, which barely extends above 1 eV, emission profiles in the various tokamaks are spread in the temperature scale up to about 10 eV. A heating mechanism for the cold atoms produced in the plasma boundary was proposed by Hey *et al* [79], which leads to the order of temperatures in the observed domain. Cold atoms, formed in excited states with temperatures as low as 0.2 eV, may be heated by atom–ion elastic scattering with the background deuterons with an assumed temperature in the 100–200 eV range. The collisional heating time for the Balmer-α lines is close to the radiative lifetime of the upper level (about 0.01 μs).

This process leads to an asymptotic temperature rise as a function of time t, from the initial T_0,

$$T = T_\mathrm{f} - (T_\mathrm{f} - T_0)\exp(-\lambda_\mathrm{c} t)\,,$$

with the collisional heating rate

$$\lambda_\mathrm{c} = \frac{16}{3\sqrt{\pi}}\alpha c n_\mathrm{f}\frac{M_\mathrm{r}}{\Sigma M}\sum_s f(s)\left(\frac{\alpha_\mathrm{pol}^{(s)}}{2}\right)^{2/(s-1)}\left[\frac{m_\mathrm{e}}{M_\mathrm{f}}\left(\frac{kT_\mathrm{f}}{E_\mathrm{H}}\right)\right]^{(s-3)/(2s-2)}.$$

The latter depends linearly on the density n_f of the background 'field' deuterons and depends on the atomic dipole and quadrupole polarizabilities $\alpha_\mathrm{pol}^{(s)}$ with $s = 4, 6$ respectively. The other symbols bear their usual meaning or are explained in detail in [79]. One cannot stress enough that $\alpha_\mathrm{pol}^{(4)}$ depends strongly on the principal quantum number ($n = 1$ or 3 in the present discussion). Calculated rate coefficients for the elastic scattering in D^+–$D(n = 1)$ collisions lie around 2.0×10^{-8} to 6.0×10^{-8} cm^3 s^{-1} depending on the initial temperature of the neutrals, values which are relatively high on the scale of other relevant atomic processes. *Heating proceeds until the process is terminated by radiative decay or ionization*. Figure 15 reflects the fate of cold hydrogen or deuterium atoms with an initial temperature of 0.2 eV: the attained temperatures are shown against deuteron temperature in the 30–270 eV range. The atoms responsible for H_α or D_α emission indeed attain values between 1 and 10 eV as shown in the right-hand picture.

Those in the ground state (left part of the figure) strikingly display temperatures between 0.2 and 1 eV only, as expected. Although this model was derived subject to a number of simplifications and can certainly be refined, the extent of agreement of both results with most of the observations makes the proposed mechanism a serious candidate for subsequent heating of cold products of molecular dissociation.

4.3. Recycling models and numerical codes—EIRENE

Recycling of atoms and molecules off material surfaces is typically a linear transport process. Self collisions between recycled atoms and molecules can often be ignored; hence neutral densities and fluxes scale linearly with the source strength, i.e. with the ion flux onto target surfaces. Neutral mean free paths are typically comparable or even larger than plasma gradient lengths (centimetres); hence fluid or even diffusion approximations are not justified. The governing linear transport equation, with realistic boundaries and a sufficiently complete set

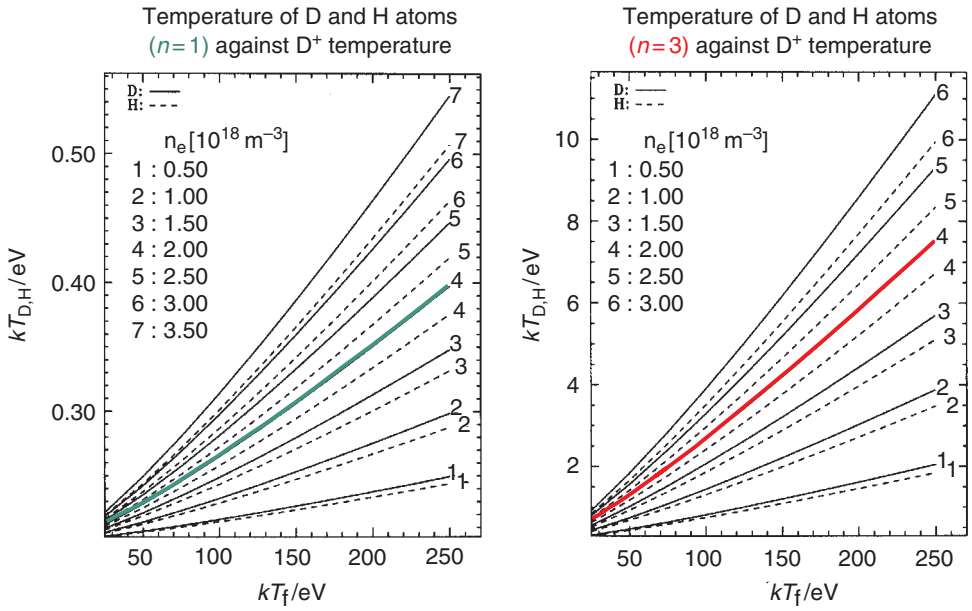

Figure 15. Temperature of deuterium and hydrogen atoms versus temperature of the background deuterons.

of atomic and molecular processes, usually has to be solved by Monte Carlo codes, such as the EIRENE code [80].

4.3.1. Transport equilibrium The characteristic length scale of the recycling process is the gradient length of plasma density and temperature, typically one or a few centimetres. Neutral particle velocities are typically in the range of 10^3–10^5 m s^{-1}. Reaction rate coefficients vary strongly with T_e, but 10^{-8} cm^3 s^{-1} is a typical value. Densities vary from 10^{10} (far SOL) to 10^{14} cm^{-3} (MARFEs, detached divertors), hence neutral particle transport timescales vary over a wide range, and mean free paths range from 10^3 to 10^{-3} m, often within the same discharge. Therefore, recycling hydrogen particles are typically not in an equilibrium determined by collisional and radiative processes, but, instead, in a type of transport equilibrium. However, timescales which are fast compared to the transport timescale need not be fully resolved in a transport calculation; often a kind of combination of many fast processes (transitions between highly excited states) into one single effective slower process, such as an effective ionization, dissociation, etc, can be utilized. In plasma edge modelling, these are usually referred to as collisional-radiative rate coefficients, although no collisional radiative equilibrium is implied here.

This partitioning into slow and fast processes is well understood for hydrogen atoms, and leads to great simplifications. In this case, it is usually clear on physical grounds which species change their populations rapidly in comparison to transport timescales, and which do not. This simple picture is made more complicated if molecules are included and a rather detailed analysis of 'slow' and 'fast' species is needed [81].

4.3.2. Atomic data Suitable effective rate coefficients for dissociation, dissociative excitation, ionization, dissociative recombination, etc, for a mixture of hydrogen atoms and molecules in

a bath of plasma electrons and ions, have first been derived by Sawada and Fujimoto [82]. A most recent contribution to the use of the current database for Monte Carlo transport modelling, e.g. for the EIRENE code, with various extensions such as isotopic effects, energy dependence in heavy particle collisions, resolution of vibrational states, has been given by Greenland [73, 81] (CRMOL, Collisional-Radiative model for MOLecular hydrogen) for zero-dimensional plasma chemistry models, and by Wünderlich [72] in a format suitable for kinetic particle transport models, as the one applied in the next section. It is perhaps worth pointing out that the treatment of molecules presents another complication not found in atoms: unless hyperfine effects are important, the excitation spectra of H and D are identical. However, the vibrational and rotational spectra of H_2 and D_2 are very different, so in the case where molecular processes play a role, H_2 and D_2 may behave very differently.

Furthermore, some of the technical details of the inclusion of molecular reactions into EIRENE are made more complicated by the larger number of processes available to molecules. This, and the larger number of slow species (see above), complicates but does not prevent the modelling of molecule-rich plasma into EIRENE. The atomic and molecular database currently linked to EIRENE can be consulted on the EIRENE domain [80].

4.3.3. Sample application For a series of plasma conditions, detailed model validation applications of the B2-EIRENE code have been carried out for TEXTOR by Gray *et al* [83], with the ALT II pump limiter (a toroidal belt limiter which can be seen in figure 2(*a*)) located 45° underneath the outer mid-plane. Figure 16 shows the ionization pattern of recycling atoms and molecules near the limiter, i.e. the spatial distribution of recycling particle sources for a low-density, ohmically heated plasma. The colour code is made equidistant on a logarithmic scale. In this specific case, about 60% of the re-ionization occurs through ionization of atoms, 40% through dissociation of molecular ions. The radial profile of the neutral atom density near the first wall in the outer mid-plane—which can already be guessed from the same figure—is presented in readable form on the right side. It is in good agreement with the radial profiles measured by laser-induced fluorescence at L_α, since the electron impact excitation is too low to resort to emission signals. For these conditions, the atomic density peaks around $8 \times 10^{15}\ m^{-3}$ in the scrape-off layer.

4.4. Need for accurate data

While a great deal of collisional data is needed to model the behaviour of molecules[1], some processes can already be identified as particularly important. For example, the main problem with analysing Fulcher band spectroscopy is the uncertainty in the excitation processes which contribute to the population of the initial Fulcher state ($d\,^3\Pi$). This state is populated by electron impact excitation from the ground state, both directly and indirectly. A significant indirect route goes *via* the $n = 2$ states, and calculations using data available at present suggest that the main part of the $d\,^3\Pi$ population comes from a two-step excitation *via* the $c^3\Pi$ state. However, these calculations do not use vibrationally resolved cross sections and there is good reason to believe that the influence of the $c^3\Pi$ state is strongly dependent on which vibrational levels are excited—radiative lifetimes and decay channels vary widely over the vibrational manifold. These lifetimes and energies are also isotopomer-dependent.

In contrast to the situation with triplet states, accurate, vibrationally resolved electron impact cross sections for the $n = 2$ and some $n = 3$ and $n = 4$ singlet states are now available [84]. Although the published results only presented cross sections vibrationally resolved for

[1] As we have already said, all the data are needed for D_2, D_2^+, HD, HD^+ as well as H_2, H_2^+, etc. In fact in many cases, for fusion plasma research, D_2 is more important than H_2. It is hoped that tritium will eventually be important as well.

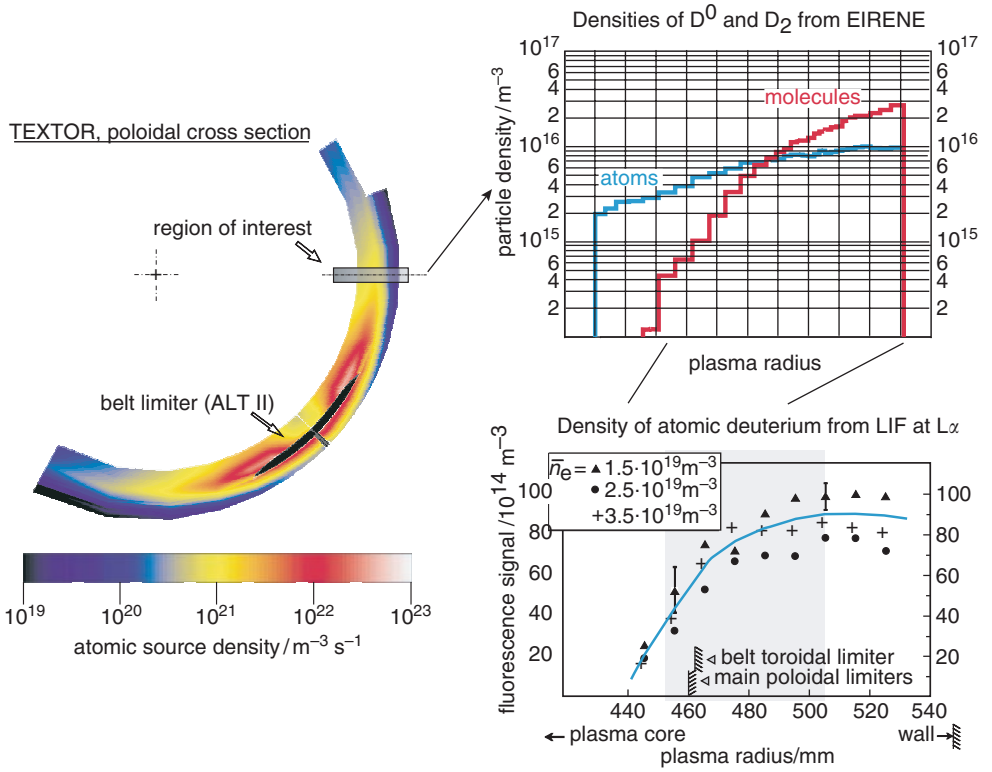

Figure 16. *Left*: Spatial distribution of recycling particle sources near the ALT II toroidal limiter blade. *Right*: Comparison of the atomic densities profiles in the outer mid-plane from EIRENE (top) incorporating molecular processes as in [72] with (bottom) the densities measured by LIF in the vicinity of the first wall, i.e. liner, of TEXTOR (ohmic shots [44]).

the initial state, the data had been computed for all $v \rightarrow v'$ transitions, and are available. In addition, useful vibrational state and mass scaling laws are known.

Molecular potential curves are known to high accuracy for many states, and can be determined for many more. They form the basis for the calculation of Franck–Condon factors, which in some cases are very sensitive to the exact form of the potential [85], and, unlike the potential curves, are strongly mass dependent. A set of reference curves would enable consistent Franck–Condon factors for all the isotopomers to be readily derived, and thereby improve our analysis of vibrationally resolved transitions. For additional information on the molecular processes and on the corresponding cross sections, the interested reader may consult [86–92].

Little has been said about the hydrogen molecular ion H_2^+. However, in contrast to H^+, it has a complex vibrational, rotational and electronic structure, and therefore electron–H_2^+ collisional data are complex. Vibrationally resolved dissociative recombination cross sections are particularly important, since this is a rapid process and, as we have seen, leads to atomic hydrogen in excited states. At the lowest temperatures discussed here, H_3^+, D_3^+ are also likely to be plasma constituents, and models will thus have to include their effects.

Finally, the role of *rotational* as well as vibrational excitation will need to be examined, particularly since work on molecular emission from graphite suggests that molecules may leave the plasma-facing surfaces in vibrationally and highly rotationally excited states [93].

This is, of course, only a list of present needs. However, since many can be satisfied by modern theoretical and/or experimental methods, it is to be hoped that modelling of molecular as well as atomic hydrogen in plasmas will progress rapidly. Administration of a minimal set of molecular data is foreseen under the aegis of ADAS [94, 95].

5. Summary and outlook

It has been shown that, although the expected plasma temperature is much higher in the vicinity of plasma-facing surfaces in the main chamber of a tokamak than in the divertor region, molecules combining all available hydrogen isotopes may be heavily involved in both cases, with recorded penetration depths in the 10 mm range. They do interfere with the evaluation of the hydrogen fluxes, since the collected Balmer photons are emitted by atoms which may either be released directly from the surface of plasma-facing components or find their origin in the dissociation of such molecules, set free from the very same areas under specific conditions. One of the main recent results is the emergence of a class of recipes to account quantitatively for the presence of molecular fluxes. In analogy with the conversion factor S/XB from photon to atomic fluxes, they rely on the determination of a similar D/XB correction, whose value depends on the local plasma parameters but can increasingly be estimated in a consistent manner. The formula applicable to such a correction is derived in the present paper. It however requires the accompanying measurement with sufficient resolution, of the order of $R \geqslant 12\,000$ over a broad spectral range (more than 40 nm!), of suitable molecular bands, two examples of which are given in the foregoing discussion.

In the same order of ideas, possible by-products of spectroscopic investigations on molecules lie in the opportunity for monitoring other plasma parameters, namely the electron density or the electron temperature, according to the available dependence of the measured molecular quantities. A further step might even be the study of local against distributed fuel inlet systems. The influence of the neutral pressure at the edge on the global quality of the confinement is now being investigated in more detail than straightforward operational edge diagrams, based on ionization alone, previously allowed.

The investigation of the detailed release mechanisms for hydrogen is still difficult in different devices owing to the local plasma conditions, which imply the interplay of completely different physical processes. But all the release mechanisms considered above have a common property: they produce hydrogen atoms with low energies, roughly below 1 eV.

On the one hand, sufficient resolving power is sometimes still lacking for an accurate analysis of *both* atomic and molecular spectra, recorded simultaneously. On the other hand, much information was gained recently in understanding dissociative excitation processes which, when occurring upon electron impact on vibrationally excited molecules, may lead to a substantial amount of atomic products with extremely low energies, in the sub-eV range. The further study of possible heating mechanisms bridges the gap between these low energies and the 1–10 eV domain which is also experimentally observed for atomic hydrogen. Finally, diagnostics with very high spectral resolution ($R \geqslant 100\,000$) may contribute in the near future to the classification of the actual release mechanisms. This knowledge is of course steadily introduced into simulation codes like EIRENE.

Among other parameters, the temperature of the surface, from which hydrogen is released, obviously plays an important role in the selection of the involved processes: the ratio of atomic to molecular contribution to the particle fluxes grows from 0 to 100%. While this temperature is an important factor, the available measurements also point out two other dependencies: the plasma density on the one hand and the choice of the material on the other. Whereas the former cannot be easily controlled independently of other global requirements on the plasma

performance, the latter has to be considered and is the subject of current investigations (graphite versus tungsten, molybdenum or tantalum).

Next-step fusion devices may well reach at definite wall locations higher temperatures for the plasma-facing surfaces, so that the molecular contribution to hydrogen release tends to vanish, but the higher densities foreseen may equally favour the opposite trend, namely an increase of the molecular fluxes!

Acknowledgments

Most results of molecular measurements on the TEXTOR tokamak are part of the PhD thesis of one of the authors (S Brezinsek). We are grateful to the University of Düsseldorf for permitting their use in the present publication. The preliminary spectral profile from the JET tokamak is given under the sole responsibility of the corresponding author who kindly acknowledges the opportunity of performing the measurements, the results of which will be submitted for later publication.

References

[1] Skinner C H *et al* 1997 *J. Nucl. Mater.* **241–243** 887–91
[2] Vietzke E and Haasz A A 1996 *Physical Processes of the Interaction of Fusion Plasmas with Solids* ed W O Hofer and J Roth (New York: Academic Press) p 135
[3] Davis J W and Haasz A A 1997 *J. Nucl. Mater.* **241–243** 37–51
[4] Roth J 1999 *J. Nucl. Mater.* **266–269** 51–7
[5] Kirschner A *Proc. 28th EPS Conf. Control Fusion and Plasma Phys.* (*Madeira, 2001*) p 4.089
[6] Mayer M *et al* 2000 *J. Nucl. Mater.* **290–293** 381–8
[7] Summers D D *et al* 2001 *J. Nucl. Mater.* **290–293** 496–500
[8] Federici G *et al* 1998 *J. Nucl. Mater.* **266–269** 14–29
[9] Unterberg B *et al Proc. 18th IAEA Conf. on Control Fusion* (*Sorrento, Italy, IAEA-CN-77/EX5/2, 2000*)
[10] Tokar M Z, Ongena J, Unterberg B and Weynants R R 2000 *Phys. Rev. Lett.* **84** 895–8
[11] Messiaen A *et al Proc. 28th EPS Conf. Control Fusion and Plasma Phys.* (*Madeira, 2001*)
[12] Strachan J D 1999 *Nucl. Fusion* **39** 1093–6
[13] Osborne T H *et al* 2001 *J. Nucl. Mater.* **290-293** 1013–17
[14] Kallenbach A *et al* 1999 *Plasma Phys. Control Fusion* **41/12B** B177–B189, see section 6, p B187
[15] Samm U and the TEXTOR Team 1999 Hydrogen recycling in *Progress in Plasma-Wall-Interaction Research—Contributions from TEXTOR-94, Plasma Phys. Control Fusion* **41** B57–B76
[16] McCracken G M and Stott P E 1979 Recycling in *Plasma-Surface Interactions in Tokamaks, Nucl. Fusion* **19/7** 889–981
[17] Harrison M F 1986 *Physics of Plasma-Wall Interactions, in Controlled Fusion* ed D E Post and R Behrisch (New York: Plenum)
[18] Vietzke E *Proc. 1st WHYPE Conf. (**W**orkshop on **Hy**drogen in the **P**lasma **E**dge) (Jülich 2000) Contrib. Plasma Phys.* submitted
[19] Verbeek H 1986 *J. Phys. E: Sci. Instrum.* **19/11** 964–70
[20] Verbeek H *et al* 1990 *Plasma Phys. Control Fusion* **32/8** 651–8
[21] Breton 1978 *Spectroscopy in the Vacuum-UV TFR-report*
[22] Fenstermacher M E *et al* 1997 *J. Nucl. Mater.* **241–243** 666–71
[23] Wenzel U *et al* 1999 *J. Nucl. Mater.* **266–269** 1252–6
[24] Behringer K and Fantz U 2000 *New J. Phys.* **2** 23.1–23.19
[25] Bogen P 1993 *Physica Scripta* **T47** 102–9
[26] Lindner P private communication
[27] Hey J D *et al* 1996 *Contrib. Plasma Phys.* **36** 583–604
[28] Mertens Ph and Pospieszczyk A 1999 *J. Nucl. Mater.* **266–269** 884–9
[29] LPX 315i (Lambda Physik, D-37079 Göttingen) and Precision-Scan DA (Sirah Laser, D-41564 Kaarst)
[30] Mahon R *et al* 1979 *IEEE J. Quant. Electron*. **15/6** 441–51
[31] Mertens Ph and Bogen P 1987 *Appl. Phys.* A **43** 197–204
[32] Brezinsek S *et al Proc. 1st WHYPE Conf. (Jülich 2000) Contrib. Plasma Phys.* submitted

[33] Hintz E and Schweer B 1995 *Plasma Phys. Control Fusion* **37** A87–A101
[34] Schweer B, Brix M and Lehnen M 1999 *J. Nucl. Mater.* **266–269** 673–8
[35] Krasheninnikov A *et al* 1997 *J. Nucl. Mater.* **241–243** 283–7
[36] Reiter D *et al* 1997 *J. Nucl. Mater.* **241–243** 342–8
[37] Fantz U, Reiter D, Heger B and Coster D 2001 *J. Nucl. Mater.* **290-293** 367–73
[38] Fantz U 2000 Deutsche Physikalische Gesellschaft, *Verhandl. DPG (VI)* **35** 1001
[39] Samm U *et al* 1989 Velocity distributions of hydrogen atoms ... in *Plasma Edge Physics in the TEXTOR Tokamak*, *J. Nucl. Mater.* **162–164** 24–37
[40] Mertens Ph and Bogen P 1989 *Proc. 16th Eur. Conf. on Controlled Fusion and Plasma Phys.* **13B/III** (*Venice*) 983–6
[41] Reiter D, Bogen P and Samm U 1992 *J. Nucl. Mater.* **196–198** 1059–64
[42] Janev R K *et al* 1987 *Elementary Processes in Hydrogen–Helium Plasmas* (Berlin: Springer) 326 pp
[43] Hey J D, Chu C C and Hintz E 2000 *Contrib. Plasma Phys.* **40** 9–22
[44] Mertens Ph and Silz M 1997 *J. Nucl. Mater.* **241–243** 842–7
[45] Sergienko G *et al* 2001 *J. Nucl. Mater.* **290–293** 720–4
[46] Condon E U 1928 *Phys. Rev.* **32** 858–72
[47] Baonian Wan *et al* 1999 *Nucl. Fusion* **39** 1865–9
[48] Kubo H *et al* 1998 *Plasma Phys. Control Fusion* **40** 1115–26
[49] Guirlet R *et al* 2001 *Plasma Phys. Control Fusion 43* 177–94
[50] Escarguel A *et al* 2001 *J. Nucl. Mater.* **290–293** 854–8
[51] Escarguel A *et al Proc. 1st WHYPE Conf.* (*Jülich* 2000) *Contrib. Plasma Phys.* submitted
[52] Koubiti M *et al Plasma Phys. Control Fusion* submitted
[53] Guirlet R *et al* 2001 *Proc. 28th EPS Conf. Control Fusion and Plasma Phys.* (*Madeira, 2001*) *Europhys. Conf. Abstracts* p 1.048
[54] Hutchinson I H 1990 *Proc. IEEE 13th Symp. Fusion Eng.* vol 1 (*Piscataway*) p 13
[55] Welch B L 2001 *et al Phys. Plasmas* **8** 1253–62
[56] Korotkov A private communication
[57] Brix M 2001 *Proc. 28th EPS Conf. Control Fusion and Plasma Phys.* (*Madeira, 2001*) *Europhys. Conf. Abstracts* p 1.101
[58] KY6, Li-Beam Diagnostic in *JET Data Handbook, Guide to Diagnostics*, JET-EFDA Org., *European Fusion Development Agreement* 2000
[59] Stangeby P C 2000 The Plasma Boundary of Magnetic Fusion Devices *IOP Plasma Physics Series* ed P Stott and H Wilhelmsson 717 pp
[60] Pospieszczyk A 1993 *Atomic and Plasma-Material Interaction Processes in Controlled Thermonuclear Fusion*, ed R K Janev and H W Drawin (Amsterdam: Elsevier) pp 213–42
[61] Fantz U and Heger B 1998 *Plasma Phys. Control Fusion* **40** 2023–32
[62] Heger B, Fantz U, Behringer K and AUG Team 2001 *J. Nucl. Mater.* **290–293** 413–17
[63] Brezinsek S *et al* 2001 *Proc. 28th EPS Conf. Control Fusion and Plasma Phys.* (*Madeira, 2001*) *Europhys. Conf. Abstracts* p 5.093
[64] Freund R S, Schiavone J A, and Crosswhite H M 1985 *J. Phys. Chem. Ref. Data* **14/1** 235–383 and Wavelengths *in* App. C: *Lines of D2*... by Dieke *et al*—AIP Doc. No. JPCRD-14-0235-627, Am. Inst. Phys.
[65] Franzen P and Vietzke E 1994 *J. Vac. Sci. Technol.* A **12** 820–5
[66] Pospieszczyk A *et al* 1999 *J. Nucl. Mater.* **266–269** 138–45
[67] Brezinsek S *et al Proc. 1st WHYPE Conf.* (*Jülich 2000*) *Contrib. Plasma Phys.* to be published
[68] Hall R *et al* 1988 *Phys. Rev. Lett.* **60** 337–40
[69] Fantz U, Heger B and Wünderlich D 2001 *Plasma Phys. Control Fusion* **43** 907–18
[70] Brezinsek S, *Jül-report* (Forschungszentrum Jülich, 2002) submitted
[71] Behringer K 1987 *J. Nucl. Mater.* **145–147** 145–53
[72] Wünderlich D 2001 *Report IPP-Garching* 10/18 113 pp
[73] Greenland P T, *Report of the Research Centre Jülich, Jül-3858* (Forschungszentrum Jülich, 2001) 60 pp, ISSN 0944-2952
[74] Hirai T *et al* 2001 *Verhandl. DPG (VI)* **36/25B** 176
[75] Haasz A A and Davies J W 1995 *J. Nucl. Mater.* **223** 312–15
[76] Hey J D, Lie Y T, Rusbüldt D and Hintz E 1993 *Proc. 20th Eur. Conf. on Controlled Fusion and Plasma Phys.* (*Lisbon*) vol 17C/III pp 1111–14
[77] Hey J D 1994 *Trans. Fusion Techn.* **25** 315–25
[78] Condon E U and Shortley G H 1985 *The Theory of Atomic Spectra* (Cambridge: Cambridge University Press) 441 pp

[79] Hey J D *et al* 1999 *J. Phys. B: At. Mol. Opt. Phys.* **32** 3555–73
[80] Reiter D *et al* http://www.eirene.de
[81] Greenland P T 2001 *Proc. Roy. Soc. Lond.* A **457** 1821–39
[82] Sawada K and Fujimoto T 1995 *J. Appl. Phys.* **78** 2913–24
Sawada K and Fujimoto T 1996 *J. Appl. Phys.* **80** 606
[83] Gray D *et al* 1999 *Phys. Plasmas* **6** 2816–25
[84] Celiberto R *et al* 1999 *Phys. Rev.* A **60** 2091–103
[85] Ajello J, Shemansky D and James G 1991 *Astrophys. J.* **371** 422–31
[86] *Proc. 1st WHYPE Conf.* (*Jülich 2000*) *Contrib. Plasma Phys.* submitted
[87] Karolis C and Harting E 1978 *J. Phys. B: Atom. Molec. Phys.* **11** 357
[88] Celiberto R *et al* 1989 *Chem. Phys.* **133** 355
[89] Tennyson J and Trevisan C S *Proc. 1st WHYPE Conf.* (*Jülich 2000*) *Contrib. Plasma Phys.* submitted
[90] Snowdon K J and Tawara H 1996 NIFS-DATA-33 45 pp
[91] Urbain X *et al Physica Scripta* special issue on *Atomic and Molecular Processes in Divertor Plasma Volume Recombination*
[92] Janev R K 1999 *Proc. Conf. on Dissociative Recomb* (*Stockholm*)
[93] Meijer A H H M, Farebrother A J, Clary D C and Fisher A J *J. Phys. Chem.* submitted
[94] Summers H P and von Hellermann M 1993 *Atomic and Plasma-Material Interaction Processes in Controlled Thermonuclear Fusion* ed R K Janev and H W Drawin (Amsterdam: Elsevier) pp 87–117
[95] Atomic Data Analysis Structure, see also http://adas.phys.strath.ac.uk